Analyst

# Actuation of chitosan-aptamer nanobrush borders for pathogen sensing



| | |
|---|---|
| Journal: | *Analyst* |
| Manuscript ID | AN-ART-12-2017-002039.R2 |
| Article Type: | Paper |
| Date Submitted by the Author: | 06-Mar-2018 |





| | |
|---|---|
| Complete List of Authors: | Hills, Katherine; Texas A&M University, Biological and Agricultural Engineering<br>Oliveira, Daniela ; Texas A&M University, Biological and Agricultural Engineering<br>Cavallaro, Nicholas; University of Florida, Agricultural and Biological Engineering<br>Gomes, Carmen; Iowa State University, Mechanical Engineering<br>McLamore, Eric; University of Florida, Agricultural and Biological Engineering Department |

# Actuation of chitosan-aptamer nanobrush borders for pathogen sensing

*Katherine D. Hills*[1], *Daniela Alves De Oliveira*[1], *Nicholas D. Cavallaro*[2], *Carmen L. Gomes*[1,3*], *Eric S. McLamore*[2]

[1]Biological and Agricultural Engineering, Texas A&M University

[2]Agricultural and Biological Engineering, Institute of Food and Agricultural Science, University of Florida

[3]Mechanical Engineering, Iowa State University

[*]Corresponding Author: 2012 Black Engineering Building, Ames, Iowa – 50011; Phone: (979) 739-0050; email: carmen@iastate.edu

**KEYWORDS**: *Listeria monocytogenes*, aptamer, nanobrush, chitosan, food safety, biosensor

**ABSTRACT**: We demonstrate a sensing mechanism for rapid detection of *Listeria monocytogenes* in food samples using the actuation of chitosan-aptamer nanobrush borders. The bio-inspired soft material and sensing strategy mimic natural symbiotic systems, where low levels of bacteria are selectively captured from complex matrices. To engineer this biomimetic system, we first develop reduced graphene oxide/nanoplatinum (rGO-nPt) electrodes, and characterize the fundamental electrochemical behavior in the presence and absence of chitosan nanobrushes during actuation (pH-stimulated osmotic swelling). We then characterize the electrochemical behavior of the nanobrush when receptors (antibodies or DNA aptamers) are conjugated to the surface. Finally, we test various techniques to determine the most efficient capture strategy based on nanobrush actuation, and then apply the biosensors in a food product. Maximum cell capture occurs when aptamers conjugated to the nanobrush bind cells in the extended conformation (pH < 6), followed by impedance measurement in the collapsed nanobrush conformation (pH > 6). The aptamer-nanobrush hybrid material was more efficient than the antibody-nanobrush material, which was likely due to the relatively high adsorption capacity for aptamers. The biomimetic material was used to develop a rapid test (17 min) for selectively detecting *L. monocytogenes* at concentrations ranging from 9 to $10^7$ CFU-$mL^{-1}$ with no pre-concentration, and in the presence of other gram-positive cells (*Listeria innocua* and *Staphylococcus aureus*). Use of this bio-inspired material is among the most efficient for *L. monocytogenes* sensing to date, and does not require sample pretreatment, making nanobrush borders a promising new material for rapid pathogen detection in food.

## Graphical Table of Contents

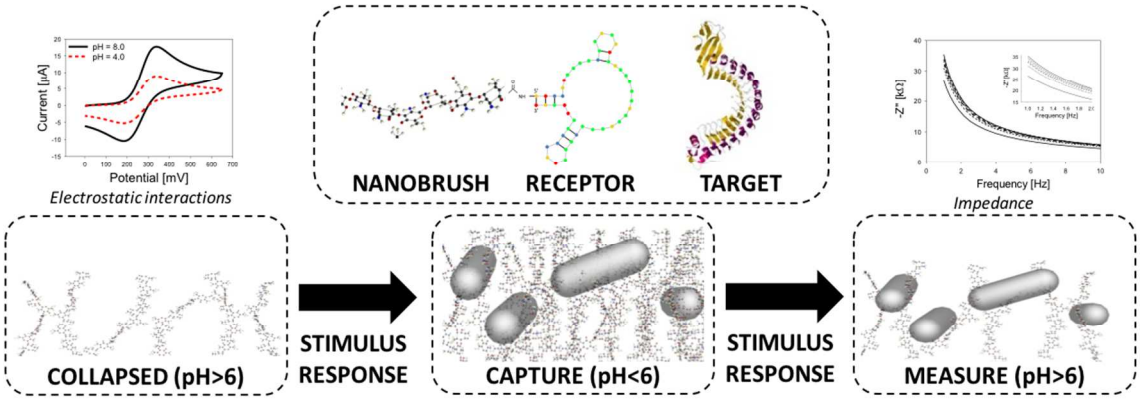


Nanobrush border sensing strategy for bacteria capture uses a combination of receptor-target binding and electrostatic interactions during stimulus-response actuation.

## Introduction

*Listeria monocytogenes* is one of the top three causes of death from foodborne illness in the world[1, 2]. Within the U.S., *L. monocytogenes* has been a persistent problem since the 1980s and the number of food recalls related to *Listeria* contamination has increased since implementation of the food safety modernization act (FSMA) in 2011[3]. *Listeria* is a ubiquitous species in water/soil and is transmitted to humans when contaminated water/soil comes into contact, whether directly or indirectly, with food meant for human consumption. *L. monocytogenes* can proliferate under low moisture content, high salinity conditions, or at temperatures associated with common refrigerator/freezer units, which makes the organism particularly difficult to monitor in food processing environments[4]. Recent recalls of cut vegetables, frozen corn/spinach, ice cream, various juices, smoked salmon, fresh produce, nuts, and frozen vegetables have occurred due to possible *L. monocytogenes* contamination[5]. Rapid sensors for detecting *L. monocytogenes* are needed, as the economic losses due to contamination are considerable[6]. These recent recalls and economic issues are direct evidence that there is a pressing need for rapid, label-free biosensors that can be used for measuring *L. monocytogenes*.

Analysis of food pathogens such as *L. monocytogenes* in food processing environments typically utilizes culture-based techniques, forward scattering phenotyping, or indirect detection via techniques such as polymerase chain reaction (see review by Wang and Salazar[7]). These technologies are selective and accurate, but are laborious, require extensive user training, addition of reagents/labels, careful control of environmental conditions, and at least 8-24 hours for confirmation[8, 9]. Due to these technological issues, a number of biosensors and immunoassays have been developed with the aim of enhancing rapid detection (reviewed in detail by Su et al.[10]). Most modern biosensors utilize nanomaterial structures as the transducer layer (e.g.,

nanocarbon, nanometal, dichalchogenides, or hybrid materials) and one or more receptor such as proteins, peptides, or oligonucleotides[11-14]. For example, common pathogen schemes include sandwich immunoassays on carbon nanotubes[15], graphene oxide or molydisulfide sensors coated with aptamers[16, 17], gold nanoparticle-conjugated antibodies[18], and a variety of other techniques (see review by Vanegas et al.[19]). To resolve problematic issues with matrix effects from food samples, many groups have developed pre-separation and/or pre-concentration methods upstream of the sensor, such as immunomagnetic separation[20], magnetic nanoparticle separation[21], dielectrophoretic separation[22], magnetic relaxation switching[23], immunochromatography[24], acoustofluidic sorting[25], ferrofluidic manipulation[26], or hydrodynamic focusing[27]. Although the combination of pre-treatment methods with state-of-the-art rapid nano-biosensors has demonstrated success in food safety monitoring, the limit of detection (LOD) is approximately $10^2$ to $10^3$ CFU-mL$^{-1}$ in real food samples, which is not adequate for many facilities[7, 9]. Thus, there is a pressing need for simple, low cost sensor materials that can enhance nano-biosensor performance at a LOD of at least 10 CFU-mL$^{-1}$ in the food matrix (or lower) and complement standard microbial analyses by providing high throughput analysis.

In nature, there are many examples of highly selective bacteria capture by protrusions (i.e., microvilli) that undergo actuation induced by changes in local chemical and/or microfluidic conditions. For example, symbiosis between the Hawaiian bobtail squid (*Euprymna scolopes*) and a Gram-positive luminescent marine bacterium (symbiont competent *Vibrio fischerii*) is based on selective recruitment and colonization of a "light organ" covered by a ciliated brush border[28]. Remarkably, symbiont-competent *V. fischerii* represent less than 0.1% of the marine bacterioplankton population, yet juvenile animals are capable of selectively recruiting *V. fischerii*

to the light organ each day after venting 90% of the luminescent bacteria[28]. Actuation of the cilia brush border is thought to play a major role in this selective capture of *V. fischerii*[29]. There are many other examples in nature, such as the intestinal epithelium, where brush borders are involved in both cell adhesion[30] and repulsion[31], depending on specific electrostatic interactions. The high selectivity of brush borders in natural systems serves as an excellent inspiration for design and fabrication of a biomimetic material for fabricating pathogen sensors based on stimulus-response nanobrushes.

The most common stimulus-response materials that could be used for an engineered brush border system include poly(N-isopropyl acrylamide) (temperature sensitive nanobrush), ionic polymer-metal composites (charge sensitive nanobrush)[32], or chitosan (pH-sensitive nanobrush)[33-35]. Among these materials, chitosan (CHI) is one of the most attractive for analysis of food, as the polymer is biocompatible, low cost, and has unique stimulus-response properties that can be easily controlled[36]. Using these material properties, a variety of CHI nanocomposites have been created, with applications including: water disinfection[37], antimicrobial food coating[38], electromechanical switches and actuators[39, 40], cancer cell irradiation[41], drug delivery[42], and sensors[43].

In this work, we focus on development of a new biomimetic material for capture of pathogens (*L. monocytogenes*) in food samples using CHI nanobrushes decorated with various receptors (**Scheme 1**). We demonstrate development of a rapid, label-free biosensor based on a hybrid nanomaterial that uses actuation of CHI nanobrushes on graphene/nanoplatinum electrodes to "recruit" target cells through a combination of electrostatic interactions and receptor-cell binding. We test two different types of receptors on the nanobrush, namely a 160 kDa polyclonal IgG and a 47-mer DNA aptamer specific to internalin A, a cell surface invasion protein found on

*Listeria*. We show that the nanobrush biosensor can selectively detect *L. monocytogenes* (95% accuracy) in a food matrix over other Gram-positive cells, which represents a new breakthrough in biomimetic soft materials for sensing.

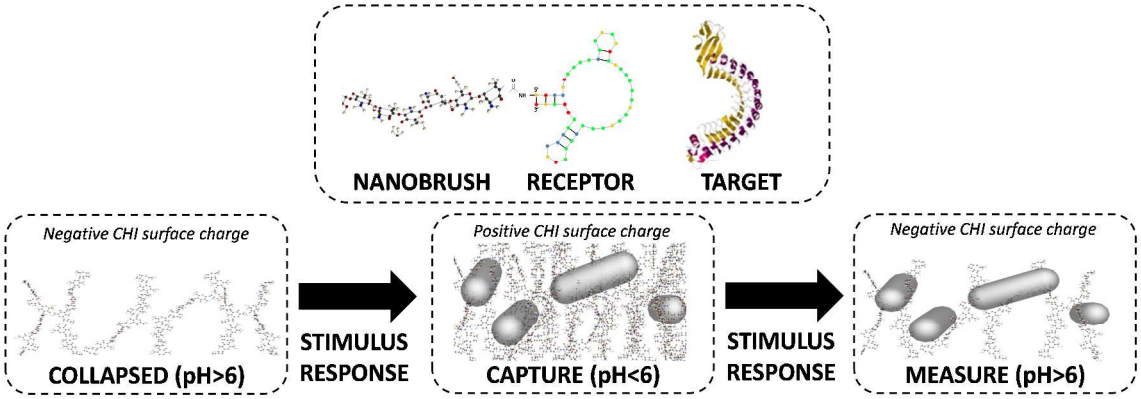


**Scheme 1**. Nanobrush sensing strategy for selective bacteria capture. Top: Stimulus-responsive chitosan (CHI) nanobrushes are decorated with receptors that bind a cell surface target (a DNA 47-mer targeting Internalin A on *Listeria monocytogenes* is shown as an example). Bottom: Nanobrush is actuated from collapsed to extended states based on pH changes. The nanobrush is first extended (pH< 6), facilitating cell capture due to a combination of electrostatic interactions and receptor-target binding, and then measurement (sensing) is conducted in the collapsed nanobrush state (pH >6).

## Results and discussion

### *Nanobrush morphology*

The reduced graphene oxide-nanoplatinum (rGO-nPt) electrode coating consisted of 118 ± 27 nm nPt fractal nodes on larger microstructures that covered the rGO surface (see supplemental Figure S1 for additional SEM images). The size of these nPt fractal clusters is similar to previous

work using similar materials[11, 44, 45]. When CHI was electrodeposited on the rGO-nPt surface (**Figure 1a**), nanobrush structures with an average diameter of 126 ± 54 nm were formed; this diameter was not significantly different than the outermost terminal cluster of the nPt ($p=0.031$, $\alpha=0.05$; see **Figure 1d** for image analysis[46]). The nanobrush length (862 ± 539 nm) varied significantly, although the precise length is difficult to determine as the underlying nPt structure is not visible in many locations (**Figure 1b**). The average diameter of CHI terminal nodes (232 ± 93 nm) was approximately twice the size of the brush width. The architecture of the CHI nanobrushes (**Figure 1c**) in this study is similar to the structure of natural brush borders on mammalian cells (intestinal enterocyte, kidney proximal tubule cells, placental syncytio-trophoblasts), which contain a longitudinal, actin-based cytoskeleton that is approximately 100 nm in diameter and 1000 nm in length[47]. In mammalian cells, these brushes are connected transversely by short, actin-binding cross filaments in the inner leaflet and the actin core filaments[48]. Our CHI nanobrushes contain a similar feature, as the CHI was cross linked with glutaraldehyde, creating a filamentous structure as shown in **Fig 1**. Hamula et al.[49] developed smaller CHI fingers than shown here by using a variable potential electrodeposition technique on gold substrate with 85% deacetylated CHI. In this work, we utilized a non-pulsed deposition technique for 5 min at 3 V using 75% deacetylated CHI, which is the most likely source of the discrepancy in brush size compared to Hamula et al.[49] as all other conditions were similar. In our preliminary studies, electropolymerization of CHI for 2 min resulted in nanobrushes, which showed no appreciable stimulus-response, and polymerization times of longer than 6 min resulted in brushes, which did not adhere well to the rGO-nPt electrodes.

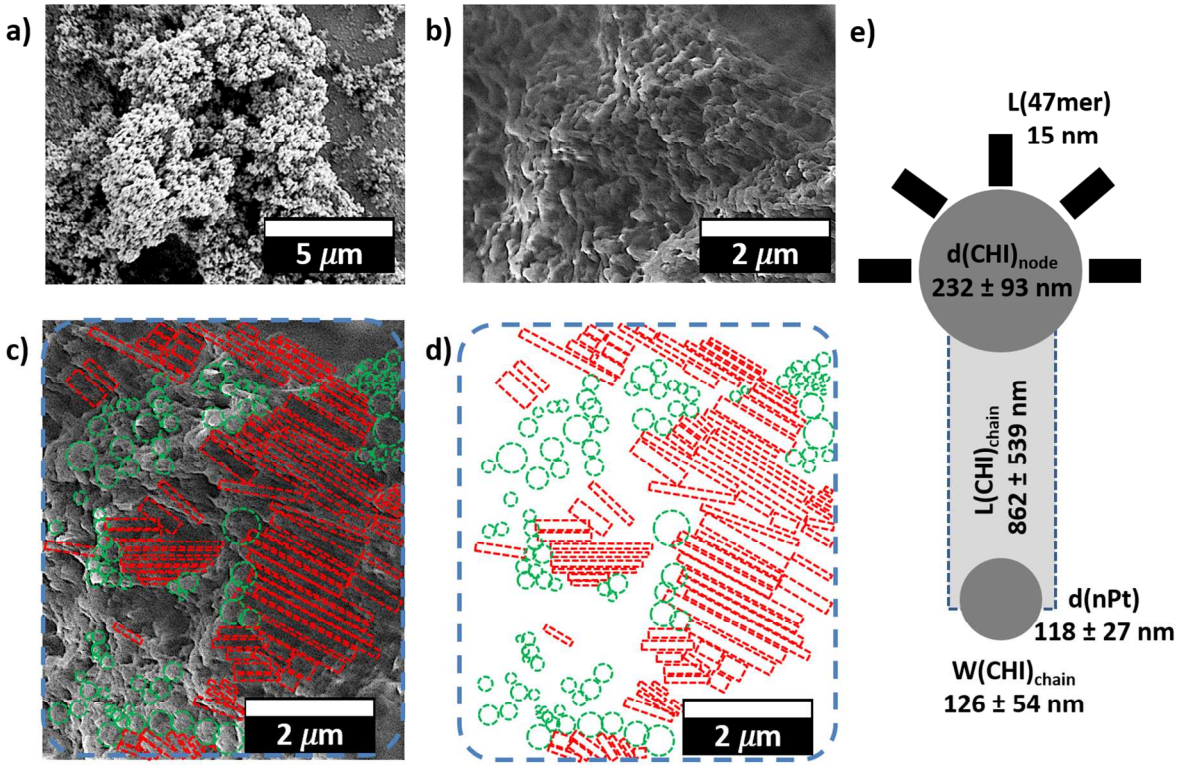


**Figure 1**. Representative SEM images of CHI nanobrushes on rGO-nPt electrodes. **a)** Low resolution image shows the formation of brush borders coating the rGO-nPt. **b)** High resolution image shows terminal nodes on the longitudinal shaft that are similar in architecture to natural brush borders. **c)** Image J analysis of CHI nanobrush features. **d)** Brush structures are shown by red rectangles and terminal nodes are highlighted as green circles (full analysis not shown). **e)** Average size of nPt and brush features based on ImageJ size analysis.

*Nanobrush electrochemistry*

Electrodeposition of CHI onto rGO-nPt electrodes increased ($P < 0.05$) the average peak oxidative current by 2.6 ± 1.4% and also increased the average electroactive surface area (ESA) by 6.1 ± 4.2%, which is similar to previous work by Martins et al.[50] and Justin et al.[51]; see supplemental Figure S2. To characterize the electrostatic interactions during nanobrush

actuation, CV curves were analyzed for three different redox probes at various pH, including a negatively charged probe ($KFeCN_6^{3-}$), a neutral probe ($C_6H_4(OH)_2$), and a positively charged probe ($Ru(NH_3)_6^{3+}$ (**Figure 2**). CHI has a pKa value that can vary between pH 6 and 7, depending upon the degree of deacetylation. The medium molecular weight CHI used here (75% deacetylated) has a pKa of 6.5[52]. When fixed to a surface this corresponds to an extended polycationic CHI conformation at pH < 6 due to increased osmotic swelling from protonation of polymeric amino groups[53, 54]. Under this condition transport of the $KFeCN_6^{3-}$ probe increases due to electrostatic interactions, $C_6H_4(OH)_2$ does not change (Debye shielding), and the $Ru(NH_3)_6^{3+}$ probe decreases due to charge repulsion/steric hindrance. Conversely, at pH > 7 polycationic amino acids on CHI are deprotonated and revert back to their stable form as hydrogen atoms are drawn toward $OH^-$ groups. Under this condition the trend in CV data is reversed since the amine groups are deprotonated and reactive, inducing steric hindrance for the $KFeCN_6^{3-}$ probe and increased current for the $Ru(NH_3)_6^{3+}$ probe. **Figure 2a-c** shows characteristic CVs for each redox probe during brush actuation, and **Figure 2d-f** shows the average peak current for replicate sensors at pH 4 or pH 8 (three repetitive cycles).

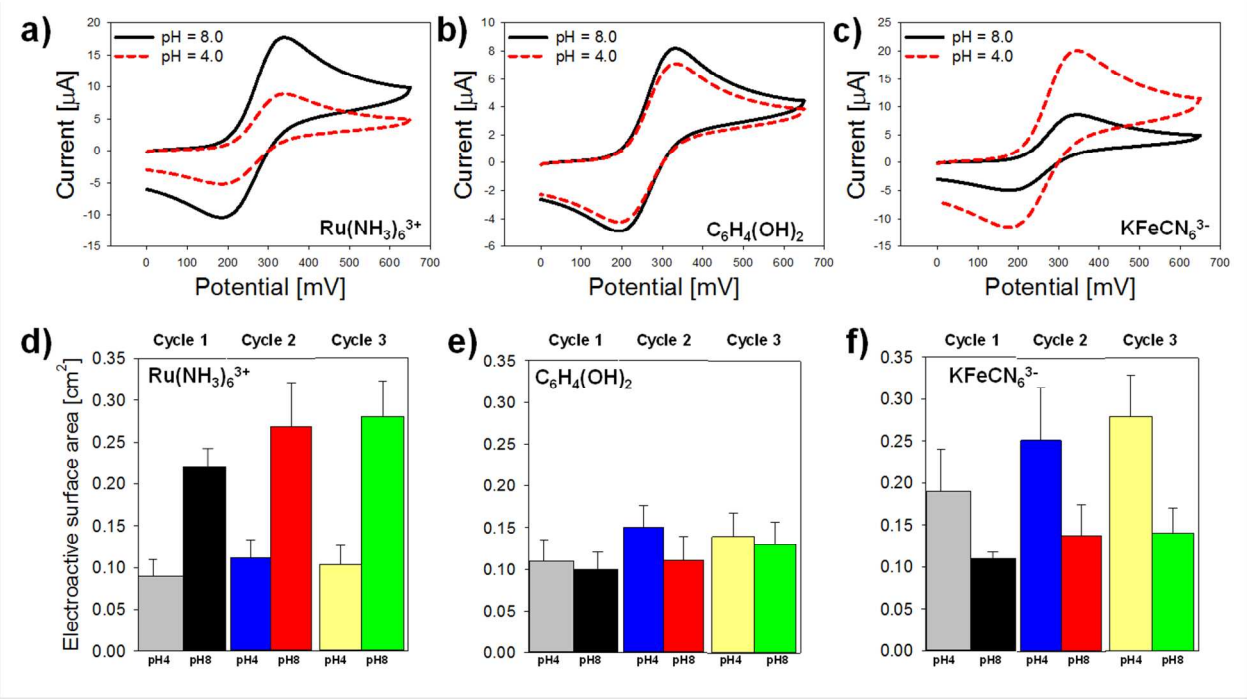


**Figure 2**. Electrostatic interactions for various redox probes during nanobrush actuation. Chitosan was deposited on rGO-nPt electrodes and CV carried out at pH 4 or 8 (25 °C) for **a)** a negatively charged probe ($KFeCN_6^{3-}$), **b)** a neutral probe ($C_6H_4(OH)_2$), and **c)** a positively charged probe ($Ru(NH_3)_6^{3+}$. In panels **d)** to **f)** average electroactive surface area (ESA) is shown for each redox probe under repeated actuation at pH 4 and pH 8 (n=3); error bars represent the standard error of the arithmetic mean.

In preliminary testing, we analyzed the efficacy of a nanoplatinum-Nafion ionic polymer metal composite (IPMC) based on the artificial cilia developed by Sareh et al.[55] as well as nanobrushes synthesized using poly-N-isopropyl-acrylamide (PNIPAAM). These nanobrushes did exhibit phase change behavior based on electrical or thermal stimulus, respectively (see supplemental Figure S3). However, in this work we only focus on CHI nanobrushes as the other materials are either cost prohibitive for food safety analysis or are not approved as non-toxic in food. In the

next section, the sensitivity of rGO-nPt electrodes with CHI nanobrushes is explored for *Listeria* detection.

*Listeria capture strategy with nanobrush actuation*

Prior to measuring bacteria capture in vegetable broth, actuation tests were carried out to determine the most efficient capture strategy based on electrochemical changes during CHI nanobrush actuation in the presence of a constant background *Listeria* concentration of $10^3$ CFU-$mL^{-1}$. With no cell capture, the average ESA (supplemental Figure S8) for the extended nanobrush conformation at pH 5 ($3.59 \pm 0.01$ X $10^{-2}$ $cm^2$) was significantly lower ($p = 0.0019$) than the collapsed conformation at pH 7 ($4.8 \pm 1.7$ X $10^{-2}$ $cm^2$) for repeated cycles using ferrocyanide as the redox probe. Similarly, the average charge transfer resistance ($R_{ct}$) and Warburg resistance (W) for the extended conformation ($R_{ct}$= 1200 ± 340 Ω; W= 1400 ± 450 Ω) were significantly higher than the collapsed conformation ($R_{ct}$= 980 ± 110 Ω; W= 1050 ± 200 Ω) ($p = 0.002$). As shown in **Fig 2**, this is primarily due to electrostatic interactions between the CHI and the redox probe, as well as changes in mass boundary layer thickness as a result of actuation. Based on measurements of average peak current and ESA, electron transport changed significantly during actuation and in the presence of *Listeria*. In **Figure 3**, the extended brush conformation at pH < 6 is noted as (EX), the collapsed brush conformation at pH > 6 is noted as (COL), the cell capture state is noted by (cap) and the electrochemical measurement step is noted by (meas). Sensing efficiency was highest when cell capture was in the extended conformation (positive CHI charge) during capture (EX/cap) followed by contraction of the nanobrush during the measurement (COL/meas). This high capture efficiency is due to the increased probability of aptamer-cell interaction in the extended phase, as well as electrostatic attraction between the CHI

and *L. monocytogenes* below pH 6. Surface charge of *L. monocytogenes* is a function of cell age, substrate type, growth media, although a detailed study by Briandet et al.[56] showed that under most conditions cells are highly negatively charged.

For the EX/cap→COL/meas strategy, the change in differential peak current (77 ± 12 μA) and $R_{ct}$ (73 ± 7 Ω) were significantly higher than the other sensing strategies ($p < 0.0001$, $\alpha = 0.05$) (**Figure 3b**). The trends in **Figure 3a-b** were consistent with impedance data at a cutoff frequency (CF) between 1 to 50 Hz (Bode plots shown in **Figure 3c**), and the maximum impedance signal was obtained at a CF of 1 Hz (**Figure 3d**). Repetitive actuation showed no degradation of the nanobrushes as shown in **Fig 2**; this reversible stimulus-response behavior is expected, as reviewed in detail by Yi et al.[54].

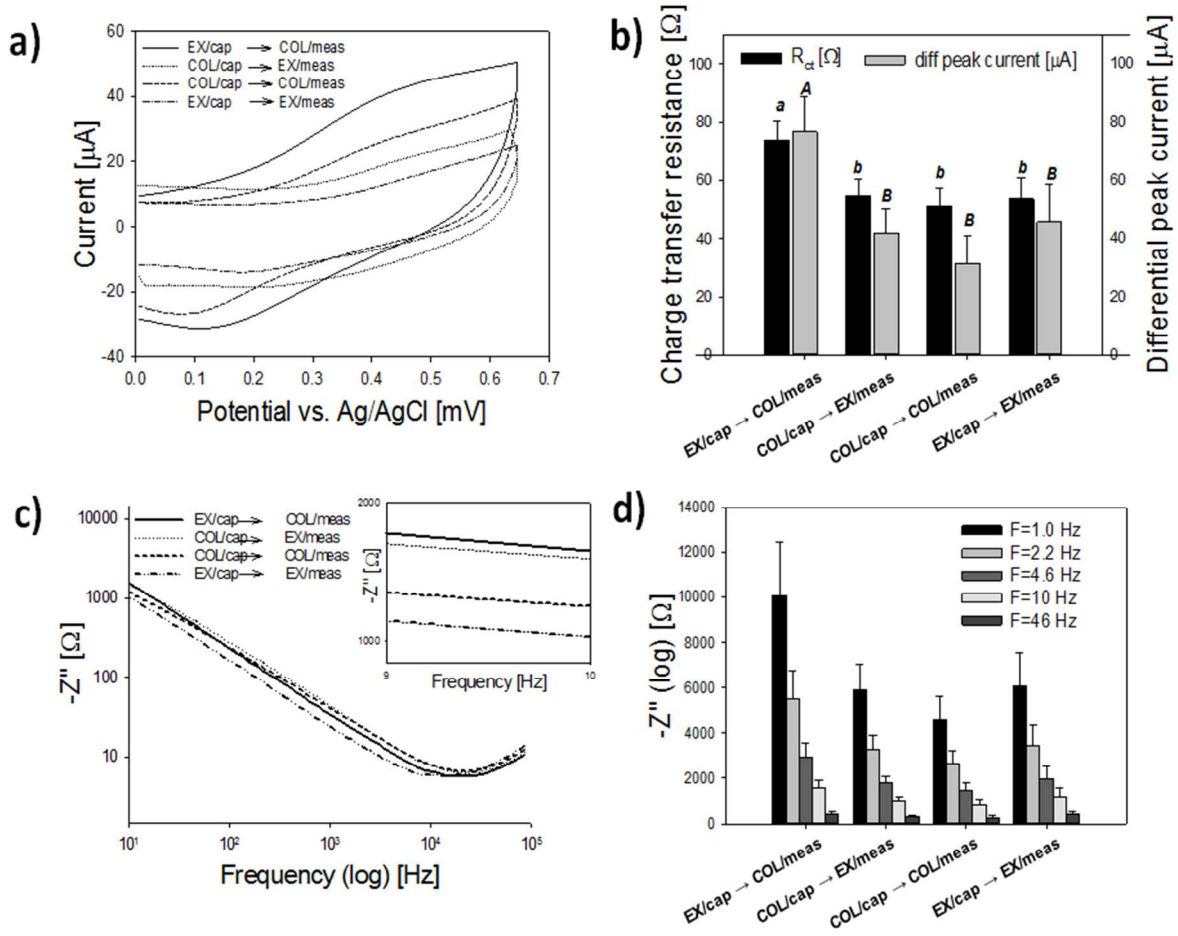


**Figure 3. a)** Representative CV (100 mV/sec) showing change in peak current for different

states of chitosan extension during *Listeria* capture ($10^3$ CFU/mL). **b)** Average change in charge transfer resistance and differential peak current during nanobrush actuation tests; lowercase letters denote statistically different groups for charge transfer resistance and uppercase letters denote statistically different groups for differential peak current (ANOVA, $\alpha$=0.05). **c)** Representative Bode plots, inset shows the impedance at a cutoff frequency of 9 to 10 Hz. **d)** Average impedance at different cutoff frequencies for various capture/measure strategies based on chitosan actuation. "EX" refers to extended state (pH 5), "COL" refers to the collapsed brush state (pH 7), "cap" refers to cell capture and "meas" refers to measurement. Error bars represent standard deviation of the arithmetic mean ($n \geq 3$).

*Biosensor characterization*

Using the EX/cap→COL/meas strategy, detection of *L. monocytogenes* was first assessed in PBS at 25 °C for rGO-nPt + CHI with each receptor. Bode plots for the aptamer nanobrush and antibody nanobrush in PBS buffer (**Figure 4a-c**) show that the impedance was approximately linear at a CF of 1 Hz at an AC potential of 100 mV. In PBS buffer, aptasensors had a higher sensitivity (3.6 ± 0.2 kΩ log-CFU-mL$^{-1}$) than the IgG sensors (3.1 ± 0.3 kΩ log-CFU-mL$^{-1}$), and the batch to batch variation was lower for replicate aptasensors; the coefficient of variation (CV) for aptasensors (0.05) was lower than all imunosensors (0.10). In vegetable broth, the sensitivity of aptasensors was not statistically different than the calibration in PBS buffer (3.8 ± 0.2 kΩ log-CFU-mL$^{-1}$), but significantly higher than immunosensors in vegetable broth (2.7 ± 0.4 kΩ log-CFU-mL$^{-1}$) or PBS buffer (**Figure 4d-f**). The behavior of the sensors in PBS buffer was linear up to $10^7$ CFU-mL$^{-1}$, but in vegetable broth the calibration curves were non-linear, with a saturation effect most likely due to non-specific binding; aptasensors saturated at $10^2$ CFU-mL (linear

range from 9.1 to $10^2$ CFU-mL), while immunosensors saturated at $10^4$ CFU-mL (linear range from 15.6 to $10^4$ CFU-mL) (**Figure 4c,f**). This non-specific binding was expected, as vegetable broth (purchased from a local grocery store) contains water, aqueous extract from cooked carrot/onion/celery, tomato paste, yeast extract, molasses, onion powder, potato flour, natural flavor, canola oil, cane sugar, and sea salt, which highlights the importance of calibrating pathogen sensors in media specific to the application of interest.

At a CF of 1 Hz, the LOD for aptasensors in buffer ($3.0 \pm 2.7$ CFU-mL$^{-1}$) was not significantly different than the immunosensors ($2.9 \pm 3.1$ CFU-mL$^{-1}$). In vegetable broth, the aptasensor LOD ($9.1 \pm 2.5$ CFU-mL$^{-1}$) was lower than the immunosensor LOD ($15.6 \pm 4.9$ CFU-mL$^{-1}$) (ANOVA, $p < 0.0001$, $\alpha = 0.05$). In buffer, LOD increased with increasing CF for both sensors, which is in accordance with expected trends based on **Figure 4** (also see supplemental Figure S9-S10). For aptasensors, increasing the value of CF did not have an effect above CF =4 Hz, with LOD values ranging from 10 to 60 CFU-mL$^{-1}$ below CF = 4 Hz, depending on the confidence interval (CI). On the other hand, immunosensors were pseudo first order at low CI (1δ) but linear at high CI (3δ). In vegetable broth, the aptasensor LOD was significantly lower than the immunosensor for all experimental conditions (ANOVA, $p = 0.005$, $\alpha = 0.05$). CF had the same positive correlation with LOD for all tests as described above, except for aptasensors at high CI (3δ). Curiously, for a CI of 99.9% the LOD decreased exponentially with increasing CF, saturating at 1 CFU-mL$^{-1}$ for a CF $\geq$ 6 Hz. As shown by Couniot et al.[57, 58], CF has a significant impact on sensitivity and limit of detection (LOD) for bacteria sensing. In our studies, the effect of CF on sensor sensitivity and LOD was dependent on media type and nanobrush configuration (details are shown in supplemental Figure S9-S10). As CF increased to 6 Hz, the LOD decreased exponentially, which was more pronounced for IgG-based sensors compared to aptasensors.

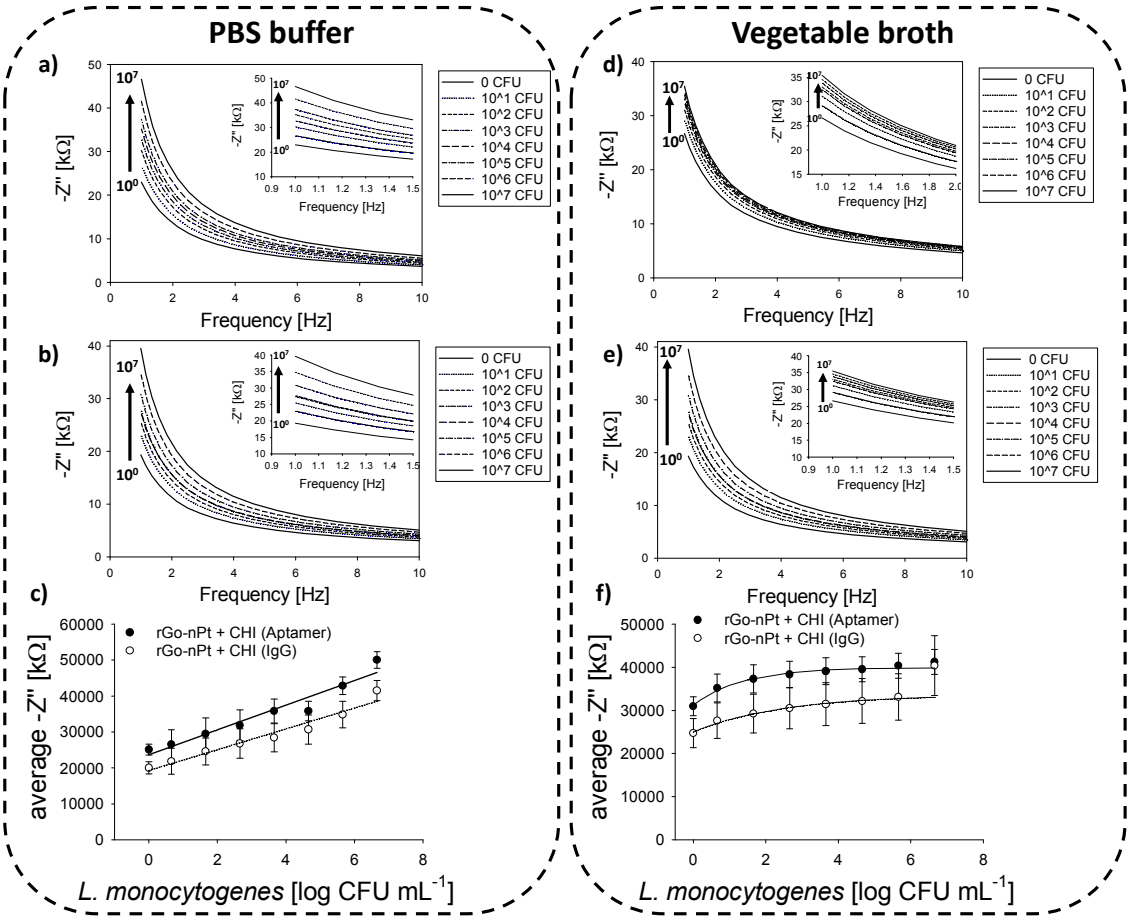


**Figure 4.** Nanobrush sensor calibration with aptamers or antibodies in PBS buffer (left) and vegetable broth (right) using the EX/cap→COL/meas. (left) Bode plots for **a)** aptamer-decorated and **b)** IgG-decorated nanobrush sensors in PBS; inset in each plot shows exploded view for a CF of 0 to 1.5 Hz at 25 °C. **c)** Linear calibration curves ($R^2$>0.98) for aptamer and IgG nanobrush sensors between $10^0$ to $10^7$ log-CFU-mL$^{-1}$ (right). Bode plots for **d)** aptamer-decorated and **e)** IgG-decorated nanobrush sensors in vegetable broth; inset shows exploded view for a CF of 0 to 1.5 Hz at 25 °C in vegetable broth. **f)** Non-linear calibration curves for aptamer and IgG nanobrush sensors between $10^0$ to $10^7$ CFU-mL$^{-1}$ (log scale), which show signal

saturation at $10^2$ CFU-mL$^{-1}$ for aptasensors and $10^4$ CFU-mL$^{-1}$ for immunosensors (calculated using SigmaPlot curve fitting enzyme kinetic module tool to obtain $K_m$ value).

To determine specificity, calibrations were repeated in the presence and absence of interfering non-target Gram-positive cells (*L. innocua* and *S. aureus*) (see supplemental Figure S11-S12). In the presence of equal background concentrations *L. innocua* or *S. aureus*, the sensitivity (0.39 ± 0.17 kΩ / log CFU-mL$^{-1}$) was significantly different than for *L. monocytogenes* detection ($p = 0.01$, $\alpha = 0.05$), which equates to 90% selectivity at equal cell concentrations. The LOD (10 ± 2 CFU-mL$^{-1}$) and response time (17 min) were not significantly different than tests performed with *L. monocytogenes* alone. Although Ohk et al.[59] showed that the 47-mer used here also binds *L. innocua* and promiscuity towards *S. aureus*, our data in the nanobrush system shows that the output signal is relatively low when compared to the capture of *L. monocytogenes*.

**Table 1** shows the performance of nanobrush sensors from this work in both PBS buffer and vegetable broth compared to other devices in the literature. The most accurate sensors to date utilize impedimetric transduction techniques. As the CF analysis above showed (see supplemental Figure S9-S10), the LOD for nanobrush aptasensors at a CI of 99.9% is 1 CFU-mL$^{-1}$ in vegetable broth at a CF $\geq$ 6 Hz. However, in **Table 1** all LOD data is reported at a CF equal to 1 Hz so that a fair comparison of different impedimetric sensors can be shown. Even at this CF, the nanobrush border sensors have one of the lowest reported LOD in real food samples at 9.1 CFU-mL$^{-1}$ and 15.6 CFU-mL$^{-1}$ for the aptasensors and immunosensors, respectively. While some sensors in literature compare with these detection limits, the nanobrush sensors have one of the fastest response times, with a total detection time of 17 minutes including sample exposure and testing.

Radhakrishnan et al.[60] developed a gold electrode-based immunosensor for *L. monocytogenes* and reported a LOD of 5 CFU-mL$^{-1}$ in tomato extract; however, the incubation time was not reported and the gold electrode (0.19 cm$^2$) was ten times larger than our electrodes. Additionally, no selectivity testing was shown and the samples required extensive pretreatment. Chemburu et. al[61] developed a 30 min amperometric sandwich immunoassay utilizing carbon dots as the platform with a LOD of 10 CFU-mL$^{-1}$ in PBS buffer, but failed to achieve the same LOD in real food samples. Ding et al.[62] developed a potentiometric sensor based on aptamer-bacteria-protamine interactions and showed a LOD of 10 CFU-mL$^{-1}$ in tris-buffered saline (TBS) with a response time of 40 minutes. While these sensors are innovative, they require a labeling step and are relatively complicated. The nanobrush border sensor is a label-free, direct analytical technique that only requires modification of the sample pH during measurement.

Other methods based on mass or optical transduction methods have also been reported for detection of *L. monocytogenes*. Piezioelectric cantilevers have a relatively high LOD ($10^2$ CFU-mL$^{-1}$) and require up to one hour for testing in food samples, not including sample pre-separation[63]. Quartz crystal microbalance sensors have been used to improve LOD to 10 CFU-mL$^{-1}$ in milk samples[64], but require at least 2 hours to complete and considerable sample pretreatment. Fiber optic sensors for interrogating aptamer binding to *L. monocytogenes* have a LOD near $10^3$ CFU-mL$^{-1}$ and analysis requires up to 4 hours[59]. Lee et al.[65] improved on this LOD and measured cell concentrations as low as 20 CFU-mL$^{-1}$ in 2 hours, but did not challenge the sensor in a food matrix. Colorimetric assays[66] are rapid (including loop-mediated isothermal amplification or LAMP), with total analysis time of less than one hour, but with poor LOD values near $10^2$ CFU-mL$^{-1}$. The LOD can be improved considerably with sample pretreatment[67], but this adds to the analysis time, which is not desirable in a food processing environment.

**Table 1**. Biosensor performance and comparison to other devices in the literature.

| | Sensor Type (E/P/M) | Sample | Sensitivity | Range [CFU-mL$^{-1}$] | Analysis Time | Reference |
|---|---|---|---|---|---|---|
| **Impedemetric** | Nanobrush Aptasensor (E) | PBS | 3.6 ± 0.2 kΩ/log CFU-mL$^{-1}$ | 3.0 to $10^7$ | 17 min | *This Work* |
| | Nanobrush Immunosensor (E) | PBS | 3.1 ± 0.3 kΩ/log CFU-mL$^{-1}$ | 2.9 to $10^7$ | 17 min | *This Work* |
| | Nanobrush Aptasensor (E) | VEG | 3.8 ± 0.2 kΩ/log CFU-mL$^{-1}$ | 9.1 to $10^2$ | 17 min | *This Work* |
| | Nanobrush Immunosensor (E) | VEG | 2.7 ± 0.4 kΩ /log CFU-mL$^{-1}$ | 15.6 to $10^4$ | 17 min | *This Work* |
| | Gold Electrode Immunosensor (E) | Tomato Extract | 1.129 kΩ cm$^2$/ CFU-mL$^{-1}$ | 5 to NR | NR | *Radhakrishnan*[60] |
| **Amperometric** | Antibody on Highly Dispersed Carbon Particles (E) | Milk & Chicken Extract | Milk: 0.0021μA/ CFU-mL$^{-1}$ (Estimated) Chicken: 0.0033 μA/ CFU-mL$^{-1}$ (Estimated) | PBS: 10 to 1.5x10$^3$ Milk: $10^2$ to 1.5x10$^3$ Chicken: 2x10$^2$ to 1.5x10$^3$ | 30 min | *Chemburu* [61] |

| | | | | | | |
|---|---|---|---|---|---|---|
| **Potentiometric** | Polycation Sensitive Membrane Electrode with Aptamers and Protamine (E) | TBS | 0.19 mV/ CFU-mL$^{-1}$ (Estimated) | 10 to NR | 40 min | *Ding*[62] |
| **Cantilever** | Piezoelectric Nanocantilever Immunuosensor (M) | Milk/ PBS Blend | 18.2 Hz/10$^{3}$ CFU-mL$^{-1}$ | 10$^{2}$ to NR | 1 hour | *Sharma*[63] |
| **QCM** | QCM with ssDNA modified Gold Nanoparticles (M) | Milk | 86.5 Hz/log CFU-mL$^{-1}$ (Estimated) | 10 to NR | Pretreatment Time: NR Test: 2 hours | *Zhou*[64] |
| **Fluorescence** | Antibody Captured/Aptamer Tagged with Fiber Optic (P) | TBS | 2850 Signal(pA)/ log CFU-mL$^{-1}$ (Estimated) | 10$^{3}$ to 10$^{9}$ | 4 hours | *Ohk*[59] |
| | Fluorescent Tagged Aptamer Sandwich Assay (P) | BHI | 9533.3 Fluorescent Intensity/log CFU-mL$^{-1}$ | 20 to 2x10$^{6}$ | 2 hours | *Lee*[65] |
| **Colorimetric** | Magnet Nanoparticle with D-Amino Acid Substrate (P) | Milk | 4.7x10$^{-5}$ %Cleavage/ CFU-mL$^{-1}$ (Estimated) | 2.17x10$^{2}$ to NR | 15 min | *Alhogail*[66] |
| | ELISA-on-a-Chip Immunosensor with Pretreatment (P) | PBS | 0.8809 Logit/ln CFU-mL$^{-1}$ | 2.4 to NR | 6 hours 20 min | *Seo*[67] |

For sensor type: E = electrochemical, P = photonic, M = mass

Range = LOD (CI = 99.9%) to the upper limit of the linear calibration plot

Time = response time (including incubation/preconcentration)

PBS = phosphate buffered solution

VEG = vegetable broth

TBS = tris-buffered saline

BHI = brain heart infusion broth

QCM = quartz crystal microbalance

NR = not reported

(Estimated) = NR sensitivities estimated by slope analysis of calibration curves

The nanobrush sensor platform developed in this work meets the demand for rapid sensors that have acceptable LOD in real food samples containing non-target cells. Importantly, the biomimetic material in this study is based on a simple stimulus-response actuation driven by local pH. Compared to the sensors listed in **Table 1**, the nanobrush sensors have the following advantages: i) the smallest physical working area (0.02 $cm^2$), ii) shortest cell capture and sensing time (17 min), iii) no requirement for label, iv) simple user operation, and v) low material cost (chitosan is an abundant natural material). We attribute the excellent performance of the sensor to the biomimetic strategy used for cell capture. Natural symbiotic systems, such as the intestinal wall or the light organ of the Hawaiian bobtail squid contain stimulus-responsive cilia brush borders that are similar in architecture and electrical properties as the sensors herein. Nanobrush borders allow for vastly increased contact surface area with microbes, and alternate surface charge during actuation. Decorating a nanobrush with a receptor such as a cell-specific aptamer adds another layer of engineered performance.

## Conclusions

The results obtained in this study confirm the basic concept of nanobrush stimulus-response as a mechanism for capturing bacteria, and this is the first study to prove that nanobrush actuation in stagnant media improves capture (relative to no actuation). In other work, various cell-

targeting receptors have been conjugated to CHI, typically as a suspended nanoparticle (NP) (reviewed by Bruno et al.[68]). Sayari et al.[69] developed CHI-aptamer NP based on carboxyethyl CHI ester and Ghasemi et al.[70] developed a similar NP based on hyaluronan-doped CHI. Similar NPs have been developed for drug delivery using antibodies (reviewed by Ragelle et al.[71]), peptides (reviewed by Layek et al.[72]), lectins (Liu et al.[73]), and folic acid (Yang et al.[74]). However, to date this chemistry has not been used to develop biomimetic brush border nanostructures for pathogen sensing, as described herein. The inclusion of CHI nanobrushes as a biomimetic brush border requires careful control over chain length, receptor adsorption, and hydrophobicity. As shown in **Figure 1** and supplemental Figure S13 (the data from 2.5 to 10 min electrodeposition time), architecture and feature play an important role on bacteria capture and sensing performance. Moreover, peak current and ESA decrease after receptors (aptamer or IgG) are conjugated to the CHI nanobrushes. Further studies are required to fully understand nanobrush actuation and ultimately optimize bacteria capture and sensing.

Although we did not study changes in fluidic transport here, Ballard et al.[75] and others have showed that actuation of microcilia can be used as a mechanism for controlling microfluidic-driven advection during bacteria capture and/or nanoparticle transport. In future designs, this principle could be combined with the sensing strategy herein to develop next generation biomimetic nanosensors that combine fluidic mixing with pathogen capture based on brush actuation. For instances, autonomous sensing and high throughput sensing could be achieved with the combination of fluidic mixing and loop-mediated microfluidic designs.

The combination of other techniques such as magneto-separation or dielectrophoresis could also assist in bacteria capture at the sensor surface to further improve the LOD. Recent work by Wang et al.[18] using magneto-separation followed by electrochemical sensing showed a LOD of

10 CFU-mL$^{-1}$ of enteric pathogen *Escherichia coli* O157:H7 in 1 hour (from sample processing to final readout). We have demonstrated a rapid method (17 min) that can selectively detect *L. monocytogenes* at concentrations ranging from 9 to $10^7$ CFU-mL$^{-1}$, which covers relevant levels for food safety analysis. Use of this bioinspired sensing material is among the most efficient capture mechanisms for *L. monocytogenes*, and does not require any sample pre-incubation or addition of exogenous reagents. The biomimetic nanostructure herein is a highly efficient platform for capturing bacteria in complex matrices, such as food samples.

## Materials and methods

### *Chemicals and reagents*

Chloroplatinic acid, 11-mercaptoundecanoic acid (11-MUA), chitosan (Medium molecular weight, 75-85% deacetylated, 200-800 cP), buffered peptone water (BPW), lead acetate, hydroquinone, and hexaaminеruthenium(III) chloride were purchased from Sigma Aldrich (St. Louis, MO). Platinum/iridium (Pt/Ir) electrodes, reference electrodes (Ag/AgCl) and Pt auxiliary electrodes were purchased from BASi Inc. (West Lafayette, IN). Glutaraldehyde, 25% (w/w) aqueous solution, and single layer graphene oxide (GO) were purchased from ACS Materials (Medford, MA). MES (2-[morpholino]ethanesulfonic acid), NHS (N-hydroxysuccinimide) and potassium nitrate were purchased from Alfa Aesar (St. Louis, MO). Sodium chloride and potassium chloride were purchased from EM Science (Darmstadt, Germany), EDC (1-ethyl-3-[3-dimethylaminopropyl]- carbodiimide) were purchased from ThermoScientific (Waltham, MA) and potassium ferrocyanide was purchased from Ward's Science (Rochester, NY). Tryptose phosphate broth (TPB) was purchased from HiMedia (Mumbai, India); buffered peptone water (BPW) and tryptic soy broth (TSB) were acquired from Becton, Dickson and Company (Sparks, MD). Petrifilm-Rapid Aerobic Count Plates were purchased from 3M (St. Paul, MN), and

potassium phosphate (monobasic) was purchased from Fisher chemicals (Pittsburg, PA). See supplemental section for specific methods used to prepare stock solutions. The DNA aptamer developed by Ohk et al.[66] for targeting *L. monocytogenes* Internalin A (47-mer, $K_d = 10^3$ CFU-$mL^{-1}$, MW 14811.63 g/mol) was purchased from Genelink (Hawthorne, NY). Polyclonal goat based anti-*Listeria* antibodies used were purchased from KPL, Inc. (Gaithersburg, MA).

*Bacteria Culture*

*Listeria innocua* (ATCC 33090) and *L. monocytogenes* (ATCC 15313) were resuscitated in TPB, and *Staphylococcus aureus* (ATCC 25923) was resuscitated in TSB. *L. innocua* is similar to *L. monocytogenes* with many of the same ecological, biochemical and genetic characteristics with the exception that *L. innocua* is a non-pathogenic strain, and therefore both *L. innocua* and *S. aureus* were used for analyzing sensor selectivity. All cells used two identical consecutive transfers and were incubated for 24 hours under aerobic conditions. Cultures were maintained on tryptic soy agar (TSA) and TSA with yeast extract (TSAYE) slants for *S. aureus* and *Listeria*; respectively, stored at 4°C for no more than 3 months. Total aerobic plate counts were measured in triplicate. Samples of the bacteria were serially diluted in BPW and plated on petrifilms (3M aerobic plate count, St. Paul, MN) and then petrifilms were incubated for 48 hours at 35 °C before counting the colony growth; results were reported as CFU-$mL^{-1}$[176]. Caution! *L. monocytogenes* and *S. aureus* are pathogenic microorganisms and must be handled using biosafety level 2 standards established by the National Institute of Health.

*Nanomaterial deposition*

Pt/Ir electrodes were cleaned prior to use following the procedures in Vanegas et al.[45] and Burrs et al.[44]. Pt/Ir electrodes were modified with a graphene-nanoplatinum "sandwich" transducer layer using the methods in Vanegas et al.[45]. In summary, a base nanoplatinum (nPt) layer was formed by electrodeposition in 1.44% (w/w) chloroplatinic acid and 0.002% (w/w) lead acetate at 10 V (constant potential) for 90 s using a BK Precision single output, programmable DC power supply (Yorba Linda, CA). Next, 2 μL of rGO stock solution (see supplemental section for details) was drop cast onto the nPt-modified electrode, dried for 1 min at room temperature, heated to 40 $^{o}$C for 30 s using a 1875 W heat gun, and spin coated according to Burrs et al.[44]. Finally, a second layer of nPt was formed at 10 V for 30 s, and sensors were stored at room temperature until used. For nanobrush deposition, nPt-rGO decorated electrodes were immersed in 10 mL of the CHI solution (prepared by mixing 1 g-CHI into 100-mL acidified DI water, previously heated to 40 $^{o}$C and pH adjusted to 5 using 2.5 M HCl solution, and stirring solution overnight) and connected to the cathode of a DC power supply with a 1 mm diameter platinum wire as the anode. CHI was electrodeposited at 3 V for 5 min according to Luo et al.[77].

To determine the effect(s) of nanobrush flexibility on aptasensor performance, the 47-mer (DNA) by Ohk et al.[59] was modified with two different functional groups; one aptamer was terminated at the 3' end with an amine, and one was terminated at 3' with a thiol group. For adsorption of DNA aptamers to nPt-rGO modified electrodes by amine-carboxyl chemistry, the surface was first carboxylated by forming a self-assembled monolayer (SAM) with 11-MUA (18 C groups). Electrodes were immersed in 500 μL of the MUA solution (see supplemental section for details) for 30 minutes at room temperature, and then electrodes were placed in 500 μL of a EDC/NHS stock solution for 2 hours at room temperature under agitation (Jantra et al.[78]). The

carboxylated nPt-rGO electrode was then immersed into a solution containing hydrated aptamers (either 50, 100, 200 or 400 nM) and allowed to adsorb for 2 h at room temperature under agitation. For adsorption of thiolated aptamers, an aliquot of stock solution (2 μL) was drop coated onto nPt-rGO electrode and dried at room temperature for 30 minutes (Vanegas et al.[45]). To conjugate aptamers to CHI, a 10% (w/v) solution of glutaraldehyde was prepared, then hydrated aptamer solution was added to a final concentration of either 50, 100, 200 or 400 nM, and CHI-modified electrodes were immersed in 500 μL of this suspension for 2 hours at room temperature under agitation. Polyclonal antibodies (IgG) were deposited on modified electrodes using carboxyl amine chemistry using the same methodology as described above; either with glutaraldehyde as a cross linker (for CHI-conjugated IgG) or with a 11-MUA SAM. All modified electrodes were stored in Tris-EDTA buffer (see supplemental) at 5 °C when not in use.

*Imaging*

Imaging was conducted using a Quanta 600 FEG scanning electron microscope (SEM) from FEI (Hillsboro, Oregon) at 5 kV and 5,000X or 10,000X magnifications. All electrodes were first coated with a 10 nm thick layer of platinum using a Cressington sputter coater 208 HR (Watford, United Kingdom); electrodes were allowed to ventilate for 30 min prior to SEM imaging.

*Electrochemistry*

All electroactive surface area (ESA) and electrochemical impedance spectroscopy (EIS) tests were performed with a 3-electrode cell set up with a Ag/AgCl reference electrode and a platinum auxiliary electrode using a CH Instruments potentiostat (CHI6044E; Austin, TX). The tests were all conducted in a 20 mL electrochemical cell (17 mL sample volume). Cyclic voltammetry (CV)

was conducted in 4 mM redox probe (either potassium ferricyanide trihydrate, hydroquinone, or ruthenium chloride) and 1 M potassium nitrate to determine ESA via the Randles-Sevcik theorem, as previously described[45, 79, 80]. CV was performed using a sweep range of 650 mV with a switching potential of 650 mV and a 30 second quiet time. For CV tests, a range of scan rates was used (50, 100, 150 and 200 mV/s). EIS was performed in 4 mM potassium ferricyanide trihydrate and 1 M potassium chloride. An initial DC voltage of 0.25 V was applied with a frequency range of 1 Hz to 100 kHz and an AC amplitude of 100 mV. All aptamer adsorption studies were performed in 4 mM potassium ferricyanide trihydrate and 1 M potassium nitrate in distilled water. For CHI actuation tests the pH of ferrocyanide solution was adjusted to pH 5 or pH 7 using a 2.5 M HCl or NaOH solution; solution pH was monitored during tests to ensure reported pH did not change by more than 0.5 pH units.

*Bacteria Detection*

EIS was used to determine the limit of detection (LOD), range and sensitivity of each biosensor. Complex plane diagrams (Nyquist plots) were used to determine the charge transfer resistance ($R_{ct}$), solution resistance ($R_s$), Warburg impedance ($Z_w$), and double layer capacitance ($C_{dl}$). Bode plots were used to determine the impedance at a fixed cutoff frequency (Z"). Change in normalized impedance ($\Delta Z_N''$) was determined from Bode plots based on equation 1, where $Z_o''$ is the measured imaginary impedance in the absence of bacteria (i.e., baseline impedance). The sensitivity was taken as the linear slope of the calibration curve prepared by plotting ($\Delta Z_N''$) versus bacteria concentration in log-CFU-mL$^{-1}$.

$$\Delta Z_N'' = \frac{Z'' - Z_o''}{Z_o''} \qquad \text{(equation 1)}$$

LOD was estimated using the 3 sigma method (99.7% confidence interval) according to equation 2:

$$LOD = \frac{\left\langle Z_o^{''} \right\rangle + 3\delta - Z_{\text{int}}^{''}}{s} \qquad \text{(equation 2)}$$

where:

$<\Delta Z_o^{''}>$ = mean imaginary impedance in the absence of bacteria [Ω];

σ = standard deviation of arithmetic mean for replicate $Z_o^{''}$ [Ω] data,

$Z_{int}^{''}$ = ordinate intercept for linear calibration plot [Ω]; and

s= sensitivity (slope) of calibration curve [Ω / log-CFU-mL$^{-1}$].

Selectivity was measured by calculating the net percent change in sensitivity and LOD in the presence of *Listeria* and another Gram-positive bacteria (*S. aureus* or *L. innocua*) for concentrations from 10 to $10^7$ CFU-mL$^{-1}$ in buffer or vegetable broth, as noted.

*Statistical Analysis*

A completely randomized design with equal replications was used in this study. All experiments were performed in triplicate as independent experiments and results were expressed as mean ± standard deviation. Data analysis was performed using SPSS software (version 21.0 for Windows). Differences between variables were tested for significance by one-way analysis of variance (ANOVA) and significantly different means ($p < 0.05$) were separated by the Tukey test.

**Conflicts of interest**

There are no conflicts to declare.

**Acknowledgements**

The authors would like to thank the National Science Foundation Nanobiosensors program (Grant No. CBET-1511953/1512659, Nanobioensing) for financial support. A special thanks to Samantha Winter for assistance with manuscript editing.

**Supplementary Information:** Experimental section (preparation of stock solutions); results and discussion section (Receptor adsorption on CHI nanobrushes)*;* supplementary figures (adsorption of aptamers or antibodies on chitosan nanobrushes, SEM images, cyclic voltammograms, Bode, Nyquist, Cottrell, and electroactive surface area plots, average oxidative peak current profile for different receptors, cutoff frequency effect on LOD and sensitivity plot).

## Notes and references

1. F. Allerberger and M. Wagner, *Clinical Microbiology and Infection*, 2010, **16**, 16-23.
2. A. H. Havelaar, F. van Rosse, C. Bucura, M. A. Toetenel, J. A. Haagsma, D. Kurowicka, A. P. J. Heesterbeek, N. Speybroeck, M. F. M. Langelaar, J. W. B. van der Giessen, R. M. Cooke and M. A. H. Braks, *PLoS One*, 2010, **5**, e13965.
3. A. B. Marks, *Harvard J. Legis.* , 2015, **52**, 126-172.
4. C. M. de Noordhout, B. Devleesschauwer, F. J. Angulo, G. Verbeke, J. Haagsma, M. Kirk, A. Havelaar and N. Speybroeck, *Lancet Infect Dis*, 2014, **14**, 1073-1082.
5. FSIS-USDA, United States Department of Agriculture. Food Safety and Inspection Service. Current Recalls and Alerts. https://www.fsis.usda.gov/wps/portal/fsis/topics/recalls-and-public-health-alerts/current-recalls-and-alerts, (accessed 11/20/2017, 2017).
6. D. C. Vanegas, C. Gomes and E. S. McLamore, *Biosens. J.*, 2016, **5**.
7. Y. Wang and J. Salazar, *Compr. Rev. Food Sci. Food Saf.*, 2016, **15**, 183-205.
8. P. Arora, A. Sindhu, N. Dilbaghi and A. Chaudhury, *Biosensors and Bioelectronics*, 2011, **28**, 1-12.
9. W. Valderrama, E. Dudley, S. Doores and C. Cutter, *Crit. Rev. Food Sci. Nutr.*, 2016, **56**, 1519-1531.
10. L. Su, W. Jia, C. Hou and Y. Lei, *Biosens. Bioelectron.*, 2011, **26**, 1788-1799.
11. S. L. Burrs, M. Bhargava, R. Sidhu, J. Kiernan-Lewis, C. Gomes, J. C. Claussen and E. S. McLamore, *Biosens. Bioelectron.*, 2016, **15**, 479-487.
12. Y. Guo, Y. Wang, S. Liu, J. Yu, H. Wang, M. Cui and J. Huang, *Analyst*, 2015, **140**, 551-559.
13. Y. Huang, X. Dong, Y. Liu, L.-J. Li and P. Chen, *J. Mater. Chem.* , 2011, **21**, 12358–12362.

14. K. Kerman, Y. Morita, Y. Takamura, M. Ozsoz and E. Tamiya, *Anal. Chim. Acta*, 2004, **510**, 169-174.
15. T. Geng, M. T. Morgan and A. K. Bhunia, *Appl. Environ. Microbiol.*, 2004, **70**, 6138-6146.
16. P. Singh, R. Gupta, M. Sinha, R. Kumar and V. Bhalla, *Microchim. Acta* 2016, **183**, 1501-1506.
17. Y. V. Stebunov, O. A. Aftenieva, A. V. Arsenin and V. S. Volkov, *ACS Appl. Mater. Interfaces*, 2015, **7**, 21727-21734.
18. Y. Wang and E. C. Alocilja, *J. Biol. Eng.*, 2015, **9**, 16.
19. D. C. Vanegas, C. L. Gomes, N. D. Cavallaro, D. Giraldo-Escobar and E. S. McLamore, *Compr. Rev. Food Sci. Food Saf.*, 2017, **16**, 1188-1205.
20. M. Uyttendaele, L. A. Jaykus, P. Amoah, A. Chiodini, D. Cunliffe, L. Jacxsens, K. Holvoet, L. Korsten, M. Lau, P. McClure, G. Medema, I. Sampers and P. R. Jasti, *Compr. Rev. Food Sci. Food Saf.*, 2015, **14**, 336-356.
21. M. Varshney and Y. Li, *Biosens. Bioelectron.* , 2007, **22**, 2408-2414.
22. B. H. Lapizco-Encinas, B. A. Simmons, E. B. Cummings and Y. Fintschenko, *Anal. Chem.* , 2004, **76**, 1571-1579.
23. Y. Chen, Y. Xianyu, Y. Wang, X. Zhang, R. Cha, J. Sun and X. Jiang, *ACS Nano*, 2015, **9**, 3184-3191.
24. S. S. Vyas, S. V. Jadhav, S. B. Majee, J. S. Shastri and V. B. Patravale, *Biosens. Bioelectron.*, 2015, **70**, 254-260.
25. S. Li, F. Ma, H. Bachman, C. E. Cameron, X. Zeng and T. J. Huang, *J. Micromechanics Microengineering*, 2017, **27**, 15031.
26. A. R. Kose, B. Fischer, L. Mao and H. Koser, *Proc. Natl. Acad. Sci. U. S. A.* , 2009, **106**, 21478–21483.
27. L. Clime, X. D. Hoa, N. Corneau, K. J. Morton, C. Luebbert, M. Mounier, D. Brassard, M. Geissler, S. Bidawid, J. Farber and T. Veres, *Biomed. Microdevices* 2015, **17**, 17.
28. S. V. Nyholm and M. McFall-Ngai, *Nat. Rev. Microbiol.*, 2004, **2**, 632-642.
29. Y. Ding, J. C. Nawroth, M. McFall-Ngai and E. Kanso, *J. Fluid Mech.*, 2014, **743**, 124-140.
30. L. C. Yu, *Tissue Barriers* 2015, **3**, e1008895.
31. K. M. Bennett, S. L. Walker and D. D. Lo, *Infect. Immun.* , 2014, **82**, 2860-2871.
32. J. Khawwaf, J. Zheng, R. Lu, A. Al-Ghanimi, B. I. Kazem and Z. Man, *Smart Materials and Structures*, 2017, **26**, 095042.
33. A. Nelson, *Nat. Mater.* , 2008, **7**, 523-525.
34. Z. Sun, W. Song, G. Zhao and H. Wang, *Cellulose*, 2017, **24**, 4383-4392.
35. Z. Sun, G. Zhao and W. Song, *Cellulose*, 2017, **24**, 441-445.
36. M. A. Elgadir, M. S. Uddin, S. Ferdosh, A. Adam, A. J. K. Chowdhury and M. Z. I. Sarker, *Journal of Food and Drug Analysis*, 2015, **23**, 619-629.
37. Y. Wang, A. G. El-Deen, P. Li, B. H. L. Oh, Z. Guo, M. M. Khin, Y. S. Vikhe, J. Wang, R. G. Hu, R. M. Boom, K. A. Kine, D. L. Becker, H. Duan and M. B. Chan-Park, *ACS Nano*, 2015, **9**, 10142-10157.
38. M. Abdollahi, M. Rezaei and G. Farzi, *Int. J. Food Sci. Technol.* , 2014, **49**, 811-818.
39. Y. Hu, W. Chen, L. Lu, J. Liu and C. Chang, *ACS Nano*, 2010, **4**, 3498-3502.
40. N. Raeis Hosseini and J. Lee, *ACS Nano*, 2015, **9**, 419-426.

41. K. H. Bae, M. Park, M. J. Do, N. Lee, J. H. Ryu, G. W. Kim, C. Kim, T. G. Park and T. Hyeon, *ACS Nano*, 2012, **6**, 5266–5273.
42. W. Zhang, K. Gilstrap, L. Wu, R. B. K C, M. A. Moss, Q. Wang, X. Lu and X. He, *ACS Nano*, 2010, **4**, 6747–6759.
43. H. N. Abdelhamid and H.-F. Wu, *J. Mater. Chem. B* 2013, **1**, 3950.
44. S. Burrs, D. C. Vanegas, M. Bhargava, N. Mechulan, P. Hendershot, H. Yamaguchi, C. Gomes and E. S. McLamore, *Analyst*, 2015, **140**, 466-476.
45. D. C. Vanegas, M. Taguchi, P. Chaturvedi, S. Burrs, M. Tan, H. Yamaguchi and E. S. McLamore, *Analyst*, 2014, **139**, 660-667.
46. R. Scorcioni, S. Polavaram and G. Ascoli, *Nature Protocols*, 2008, **3**, 866-873.
47. M. S. Mooseker, *Annu. Rev. Cell Biol.*, 1985, **1**, 209-241.
48. E. M. Danielsen and G. H. Hansen, *Biochimica et Biophysica Acta - Biomembranes*, 2003, **1617**, 1-9.
49. C. L. A. Hamula, H. Zhang, F. Li, Z. Wang, X. Chris Le and X. F. Li, *TrAC - Trends in Analytical Chemistry,*, 2011, **30**, 1587–1597.
50. A. M. Martins, G. Eng, S. G. Caridade, J. F. Mano, R. L. Reis and G. Vunjak-Novakovic, *Biomacromolecules*, 2014, **15**, 635–643.
51. R. Justin and B. Chen, *J. Mater. Chem. B*, 2014, **2**, 3759–3770.
52. J. Nilsen-Nygaard, S. P. Strand, K. M. Vårum, K. I. Draget and C. T. Nordgård, *Polymers*, 2015, **7**, 552-579.
53. T. López-León, E. L. S. Carvalho, B. Seijo, J. L. Ortega-Vinuesa and D. Bastos-González, *J. Colloid Interface Sci.* , 2005, **283**, 344-351.
54. H. Yi, L. Q. Wu, W. E. Bentley, R. Ghodssi, G. W. Rubloff, J. N. Culver and G. F. Payne, *Biomacromolecules*, 2005, **6**, 2881-2894.
55. S. Sareh, J. Rossiter, A. Conn, K. Drescher and R. E. Goldstein, *J. R. Soc. Interface* 2012, **10**, 20120666.
56. R. Briandet, T. Meylheuc, C. Maher and M. N. Bellon-Fontaine, *Appl. Environ. Microbiol.* , 1999, **65**, 5328-5333.
57. N. Couniot, A. Afzalian, N. Van Overstraeten-Schlogel, L. A. Francis and D. Flandre, *Sensors Actuators, B Chem.*, 2015, **211**, 428-438.
58. N. Couniot, D. Flandre, L. A. Francis and A. Afzalian, *Sensors Actuators, B Chem.*, 2013, **189**, 43-51.
59. S. H. Ohk, O. K. Koo, T. Sen, C. M. Yamamoto and A. K. Bhunia, *J. Appl. Microbiol.* , 2010, **109**, 808-817.
60. R. Radhakrishnan, M. Jahne, S. Rogers and I. I. Suni, *Electroanalysis* 2013, **25**, 2231-2237.
61. S. Chemburu, E. Wilkins and I. Abdel-Hamid, *Biosens. Bioelectron.* , 2005, **21**, 491-499.
62. J. Ding, J. Lei, X. Ma, J. Gong and W. Qin, *Anal. Chem.* , 2014, **86**, 9412-9416.
63. H. Sharma and R. Mutharasn, *Biosens. Bioelectron.* , 2013, **45**, 158-162.
64. H. Zhou, Z. Gao, G. Luo, L. Han, S. Sun and H. Wang, *Anal. Lett.* , 2010, **43**, 312-322.
65. S. H. Lee, J. Y. Ahn, K. A. Lee, H. J. Um, S. S. Sekhon, T. Sun Park, J. Min and Y. H. Kim, *Biosens. Bioelectron.*, 2015, **68**, 272-280.
66. S. Alhogail, G. A. R. Y. Suaifan and M. Zourob, *Biosens. Bioelectron.*, 2016, **86**, 1061-1066.
67. S. M. Seo, I. H. Cho, J. H. Kim, J. W. Jeon, E. G. Oh, H. S. Yu, S. B. Shin, H. J. Lee and S. H. Paek, *Bull. Korean Chem. Soc.* , 2009, **30**, 2993-2998.

68. J. G. Bruno, *Pharmaceuticals*, 2013, **6**, 340-357.
69. E. Sayari, M. Dinarvand, M. Amini, M. Azhdarzadeh, E. Mollarazi, Z. Ghasemi and F. Atyabi, *Int. J. Pharm.* , 2014, **473**, 304-315.
70. Z. Ghasemi, R. Dinarvand, F. Mottaghitalab, M. Esfandyari-Manesh, E. Sayari and F. Atyabi, *Carbohydr. Polym.*, 2015, **121**, 190-198.
71. H. Ragelle, G. Vandermeulen and V. Préat, *Journal of Controlled Release*, 2013, **172**, 207-218.
72. B. Layek, L. Lipp and J. Singh, *International Journal of Molecular Sciences*, 2015, **16**, 28912–28930.
73. J. Liu, L. Zhang, C. Wang, H. Xu and X. Zhao, *Mol. Biosyst.* , 2010, **6**, 954-957.
74. S. J. Yang, F. H. Lin, K. C. Tsai, M. F. Wei, H. M. Tsai, J. M. Wong and M. J. Shieh, *Bioconjug. Chem.* , 2010, **21**, 679–689.
75. M. Ballard, Z. Mills, S. Beckworth and A. Alexeev, *Microfluid. Nanofluidics*, 2014, **17**, 317-324.
76. AOAC, *Official method 990.12. Aerobic Plate Count in Foods*, 1990.
77. X. L. Luo, J. J. Xu, Y. Du and H. Y. Chen, *Anal. Biochem.* , 2004, **334**, 284-289.
78. J. Jantra, P. Kanatharana, P. Asawatreratanakul, M. Hedström, B. Mattiasson and P. Thavarungkul, *J. Environ. Sci. Health. A. Tox. Hazard. Subst. Environ. Eng.*, 2011, 1450-1460.
79. P. Chaturvedi, D. C. Vanegas, M. Taguchi, S. L. Burrs, P. Sharma and E. S. McLamore, *Biosens. Bioelectron.* , 2014, **58**, 179-185.
80. M. Taguchi, N. Schwalb, Y. Rong, D. C. Vanegas, N. Garland, M. Tan, H. Yamaguchi, J. C. Claussen and E. S. McLamore, *Analyst*, 2016, **141**, 3367-3378.

## Graphical Table of Contents

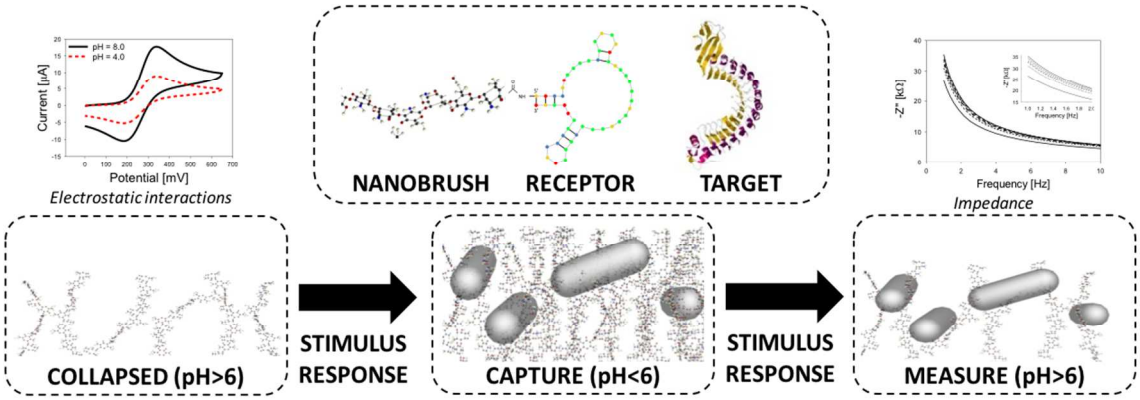


Nanobrush border sensing strategy for bacteria capture uses a combination of receptor-target binding and electrostatic interactions during stimulus-response actuation.